J MATER SCI **41** (2006) 4307–4313

Mechanical and fracture behavior of powder metalurgy processed Ti_3Al-based alloys

B. DIMČIĆ*, I. CVIJOVIĆ, M. T. JOVANOVIĆ, D. BOŽIĆ
Department of Material Science, Institute of Nuclear Sciences ≪Vinča≫, P.O. Box 522, 11001 Belgrade, Serbia and Montenegro
E-mail: bidim@vin.bg.ac.yu

O. DIMČIĆ
TCF, Mihajlo Pupin Boulevard 176, Belgarde, Serbia and Montenegro

Published online: 21 April 2006

This work considers structural and compression mechanical properties of three Ti_3Al-based alloys processed by powder metallurgy. Mechanically alloyed powders were compacted by hot-pressing to non-porous homogenous compacts. Prior to compression tests, all compacts were homogenized by a solution treatment at 1050°C ($\alpha + \beta$ region) for 1h, followed by water quenching. The compression tests were performed from room temperature to 500°C in vacuum at a strain rate of $2.4 \times 10^{-3}\,s^{-1}$. Detailed microstructural characterization has been evaluated by scanning electron microscopy (SEM), followed by electron dispersive spectroscopy (EDS) and X-ray diffraction analysis. Fracture topography was examined by SEM. The Ti_3Al-Nb alloy exhibits the highest ductility in the whole temperature range, whereas addition of Mo to Ti_3Al-Nb alloy yields the highest ultimate compression strength. A correlation between ductility and the fracture mode exists for all materials.

1. Introduction

Intermetallic compound Ti_3Al (α_2 phase) with ordered hcp structure ($D0_{19}$) is the main constituent in a single- or two phase alloys, e.g. $TiAl/Ti_3Al$ (γ/α_2). Due to their low density, good oxidation and creep resistance at high temperatures combined with high strength, these materials are promising for heat-resisting and heat-proof application in aerospace, automobile and other industries [1, 2]. However, the greatest disadvantage of these materials is their high brittleness. Recently, room temperature ductility and high temperature properties of Ti_3Al-based alloys have been improved by the addition of the β (bcc)–stabilizing elements such as Mo, Nb, V or Ta [3, 4]. Powder metallurgy processing (PM) demonstrated superior mechanical properties of titanium aluminides to those processed by conventional ingot metallurgy due to microstructural homogeneity, minimized segregation and refined grain size [5, 6]. Since the microstructure of Ti_3Al-based alloys processed by PM is sensitive to processing history, the optimization of microstructure-property relation to an appropriate PM process control becomes an important issue.

The aim of this work was to understand the influence of microstructure and alloying additions on the compression characteristics and fracture behavior at room and elevated temperatures of Ti_3Al-based alloys produced by PM process.

2. Experimental

The materials chosen for this investigation were three Ti_3Al-based powders. The nominal chemical composition of these materials is given in the Table I.

The Ti_3Al initial powder was produced by Max-Planck Institute für Metallforschung, Stüttgart, while two other powders were prepared in Institute of Nuclear Sciences "Vinča" by mechanical alloying. The mixtures consisting of Ti_3Al and Nb, and Ti_3Al, Nb and Mo powders were ball-milled (ceramic Y_2O_3 balls were used for milling) for 24 h in vacuum at 10 Pa. In the next step, the powders were hot-pressed at various temperature-pressure combinations. The optimal time and temperature of vacuum hot-pressing were determined by measuring the density of compacts by the conventional Archimedes method. The highest density (approximately 100%) corresponded to 1350°C and 4 h of annealing for all three materials. Compaction pressure in all cases was 35 MPa.

*Author to whom all correspondence should be addressed.
0022-2461
DOI: 10.1007/s10853-006-7002-0

TABLE I. Nominal chemical composition of Ti_3Al-based intermetallic powders

	Composition, at%			
Powder	Ti	Al	Nb	Mo
Ti_3Al	75	25	–	–
Ti_3Al-Nb	66	23	11	–
Ti_3Al-Nb-Mo	66	22	11	1

TABLE II. The lattice parameters of Ti_3Al phase calculated from the X-ray diffraction patterns of intermetallic powders

	Parameters (nm)		
Powder	*a*	*c*	*c*/*a*
Ti_3Al	0.5776	0.4640	0.803
Ti_3Al-Nb	0.5783	0.468	0.802
Ti_3Al-Nb-Mo	0.5807	0.4656	0.802

Prior to compression testing all compacts were subjected to the solution treatment under the protection of high purity argon atmosphere at 1050°C ($\alpha + \beta$ region) for 1 h, followed by water quenching. Compressive strength testing was conducted in the temperature range from 20 to 500°C in a vacuum chamber (vacuum was 0.1 Pa) at a strain rate of 2.4×10^{-3} s^{-1}, using rectangular specimens with dimensions $4 \times 4 \times 8$ mm.)

Specimens for scanning electron microscope (SEM) examination were prepared by standard techniques of grinding and polishing, after which the specimens were etched in a Kroll's solution consisting of 93 ml H_2O, 1 ml HF and 6 ml HNO_3.

Energy dispersive spectroscopy (EDS) and X-ray diffraction were used for the semiquantitative examinations of microstructure. The fracture surface topography was also examined by SEM.

3. Results and discussion

SEM analysis of the starting Ti_3Al powder (average size <125 μm), showed that the powder particles were nodular or irregular in shape (Fig. 1a). The other two, mechanically alloyed powders (Ti_3Al-Nb, Ti_3Al-Nb-Mo), consisted of smaller particles (average size <90 μm), irregular in shape due to the prolonged mechanical treatment in the ball-mill (Fig. 1b)

Before performing any kind of characterization it was important to attain proofs that mechanical alloying was successfully performed. X-ray diffraction patterns of powders are presented in Fig. 2a–c. Beside the peaks corresponding to Ti_3Al phase few peaks of retained elemental Nb and Mo can also be observed. The peaks of Ti_3Al are very slightly shifted in Ti_3Al-Nb, Ti_3Al-Nb-Mo powders compared to the peaks of the initial Ti_3Al powder probably due to the dissolution of alloying elements in the Ti_3Al ($D0_{19}$) lattice. The lattice parameters calculated from the X-ray patterns showed that values of *a* and *c* lattice parameters of the α_2 (Ti_3Al) phase are higher in mechanically alloyed powders than those of the pure Ti_3Al powder (Table II), which can also be taken as a proof of the dissolution of Nb and Mo into the Ti_3Al lattice.

EDS analysis (Table III) shows the quantitative evaluation of the chemical composition of the three different compacts. In the case of Ti_3Al compact the chemical composition was the same in the interior of grain as well as at the prior grain boundary. The presence of the alloying elements in the grain interior in the case of two other alloys (Ti_3Al-Nb and Ti_3Al-Nb-Mo) indicates that mechanical alloying was successfully performed. The presence of any kind of impurities such as oxygen, carbon or hydrogen was not detected.

The microstructures of solution treated compacts are shown in Fig. 3a-c. It can be noticed that the structure of all compacts is homogenous and non-porous. Fig. 3a displays the structure of Ti_3Al compact, which consists of the α_2 phase formed during previous furnace-cooling from compaction temperature (1350°C) by ($\beta \rightarrow \alpha \rightarrow \alpha_2$ transformation sequence. In the case of this alloy, solution treatment at 1050°C for 1h followed by water quenching, did not succeed to retain the ductile β phase in the structure. The other two alloys exhibit a fully transformed Widmanstätten microstucture. Fine lamellae of α_2 phase can be observed in the β phase matrix

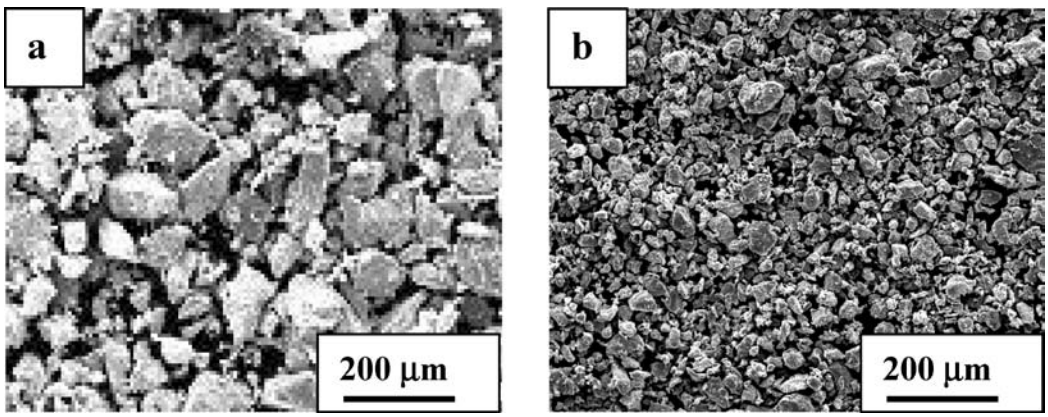

Figure 1 SEM micrograph of (a) Ti_3Al and (b) Ti_3Al-Nb-Mo powder particles.

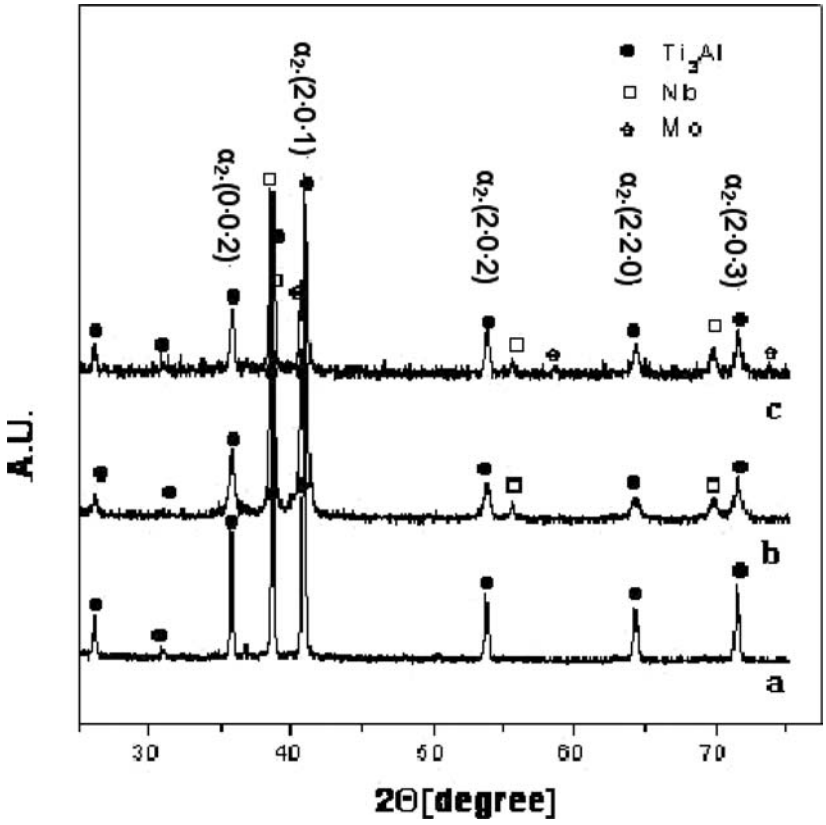

Figure 2 X-ray diffraction patterns of Ti_3Al-based powders. (a) Ti_3Al; (b) Ti_3Al-Nb and (c) Ti_3Al-Nb-Mo.

(Fig. 3b, c). This $\alpha_2 + \alpha$ two-phase structure was retained due to the presence of the β-stabilizing elements in the composition.

Distribution of chemical elements in three alloys was established by EDS analysis of solution treated specimens. This analysis clearly shows the difference in chemical composition between α_2 and β phase (Fig. 4). As it was expected, Ti is equally distributed throughout the whole structure, while the highest amount of Al is connected within the β_2 phase. As β phase stabilizers Nb and Mo are detected in the narrow areas of this phase.The mechanical properties of Ti_3Al-based alloys are strongly affected by chemical composition *via* the microstructure. The effect of these parameters on the compression strength and ductility of the Ti_3Al-based alloys at room and elevated temperatures is illustrated in Fig. 5a,b.

The ultimate compression strength (UCS) increases with increasing deformation temperature, passes through the maximum at approximately 250°C and than a decrease occurs (Fig. 5a). This behavior is essentially the same for all three alloys. Ti_3Al exhibits a strong anisotropy in strength, ductility and fracture, i.e. the basal, prism, and pyramidal slip systems are operative depending on crystal orientation and there is a great difference in the critical resolved shear stress (CRSS) for these slips and their temperature dependence. CRSS for pyramidal slip increases with increasing temperature showing an anomalous peak at around 500°C, while for prism and basal slips, after maintaining a constant value, a decrease of CRSS appears after 700 and 800°C, respectively [7]. Although in the case of this paper the material is polycrystalline, it is quite probable that the pyramidal slip, being the most operative deformation mechanism, is most effective on the appearance of UCS maximum at 250°C.

It was previously demonstrated [8] that the decrease of c/a ratio induces the decrease of the stacking density of

TABLE III. Results of the Spot chemical analysis of Ti_3Al-based alloys

	Chemical composition, *at%*							
	Ti		Al		Nb		Mo	
Alloy	Interior of grain	Grainw bondary	Interior of grain	Grain bondary	Interior of grain	Grain bondary	Interior of grain	Grain bondary
Ti_3Al	75.2	75.3	24.8	24.7	–	–	–	–
Ti_3Al-Nb	69.5	70.1	24.0	19.5	6.5	10.4	–	–
Ti_3Al-Nb-Mo	70.2	70.7	24.8	19.8	4.3	8.4	0.7	0.9

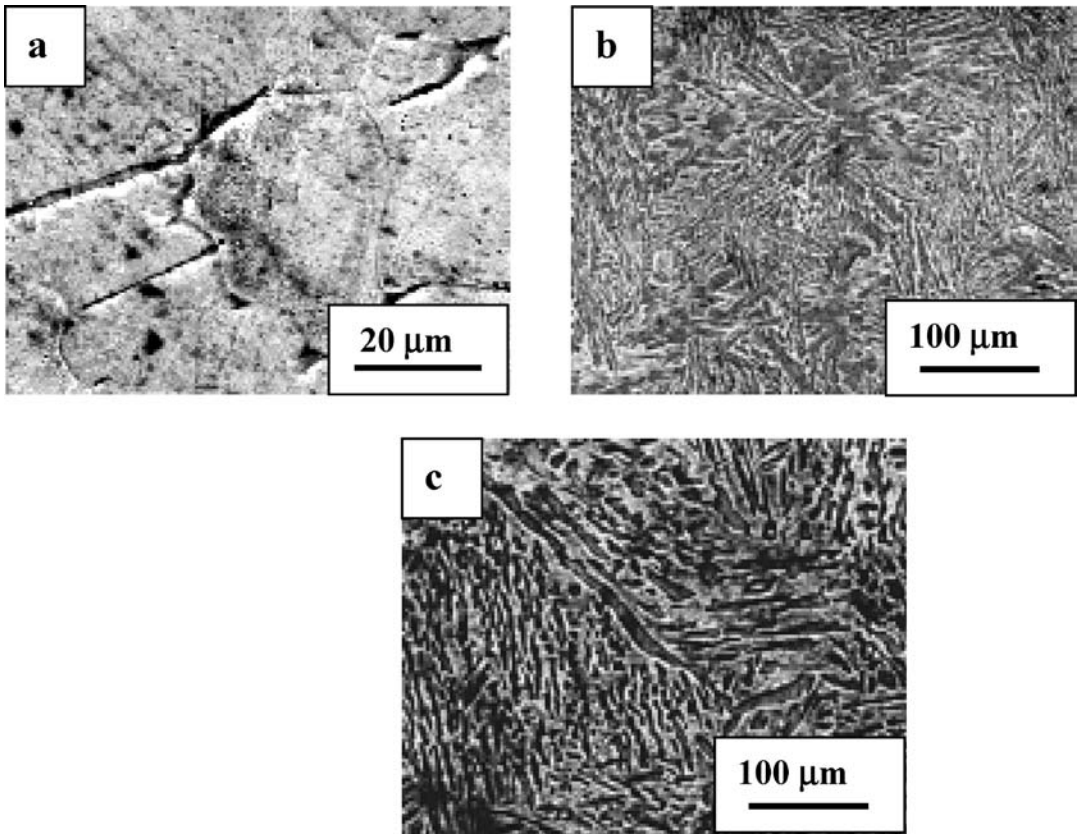

Figure 3 SEM micrograph of solution treated (annealed at 1050°C for 1h) and water-quenched compacts. (a) Ti_3Al; (b) Ti_3Al l-Nb and (c) Ti_3Al-Nb-Mo alloys.

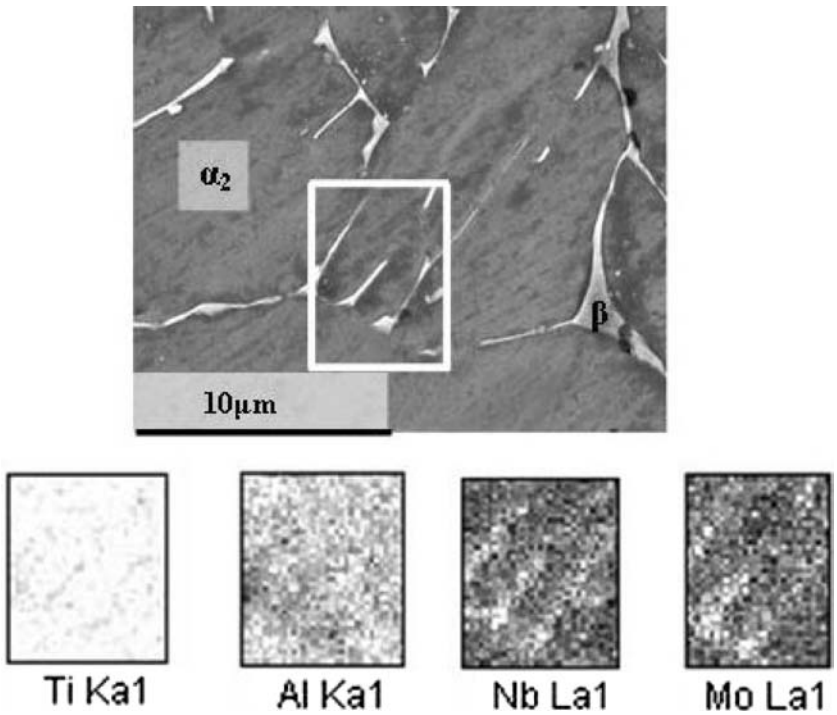

Figure 4 SEM. Microstructure and EDS analysis of chemical elements distribution in the case of solution treated (annealed at 1050°C for 1 h) and water-quenched compacts of Ti_3Al-Nb-Mo alloy.

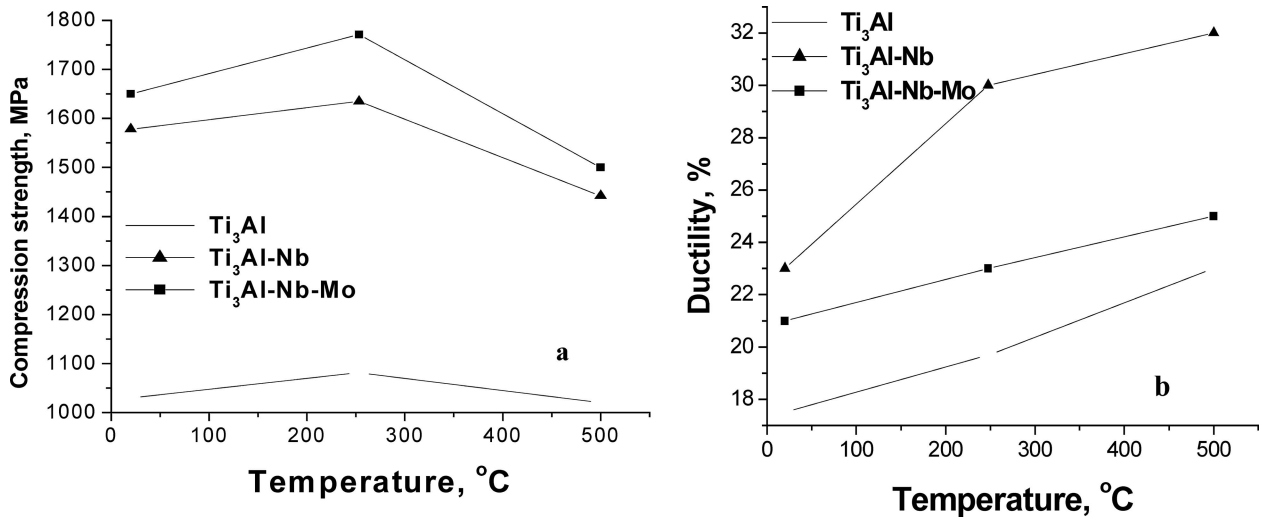

Figure 5 The effect of chemical composition on (a) compression strength and (b) ductility of different Ti_3Al-based alloys at elevated temperatures.

atoms in the basal plane in hcp lattice, and the increase of stacking in prism and pyramidal planes, which than transform into primary slip planes. This behavior is noted in the case of the examined materials, where the c/a ratio decreases in the Ti_3Al-Nb and Ti_3Al-Nb-Mo alloys compared to the pure Ti_3Al alloy (Table II). The results of Fig. 5a show that the maximum of the UCS is less in the case of Ti_3Al than those in the other two alloys. This is in the agreement with the mentioned theory and supports the idea of the supposed slip behavior of these materials. On the other hand, the addition of Mo not only stabilizes high-temperature β phase but also strengthens Ti_3Al-Nb based alloys [9], and this is well documented by the highest values of UCS of Ti_3Al-Nb-Mo alloy (Fig. 5a). Ductility increases throughout the whole temperature range for all three materials, with the highest values being exhibited by Ti_3Al-Nb alloy (Fig. 5b).

This behavior of three different Ti_3Al-based alloys can be related to their microstructure. Comparing Fig. 3a with Fig. 3b,c it seems that the effect of microstructure on UCS plays an important role, i.e. microstructure of initial Ti_3Al differs from other two alloys which multi-phase microstructures are almost the same. It is obvious that the different behavior of these alloys is the consequence of some parameters other than the morphology and the grain size. Gogia and co-workers [10] presented the results regarding the dependence of mechanical properties of Ti_3Al-Nb alloys on the amount of α_2 phase in the microstructure (Fig. 6). It can be seen that UCS and YS decrease with the increase of α_2 phase, while the ductility increases up to 30 vol.% of α_2 phase, passes through the maximum and then decrease occurs. Values of the volume fraction of α_2 and β phase for three alloys investigated in this work are presented in the Table IV. It can be observed that the amount of retained β phase increases with increase of the content of β stabilizing elements, showing the highest value for Ti_3Al-Nb-Mo alloy. This result is reasonable considering the greatest Mo β stabilizing power [11], but, in the same time, the synergetic effect of both Nb and Mo has to be considered. In view of these facts, the highest value of UCS may be expected in Ti_3Al-Nb-Mo alloy, while Ti_3Al-Nb, due to the most favorable value of α_2 volume fraction (closest to the theoretical 30 vol.%) exhibits highest values of the ductility in the whole temperature range.

Figs 7a,b shows the fracture surface of pure Ti_3Al alloy tested at room temperature and 500°C, respectively. In general, transgranular brittle fracture is the main fracture mechanism of the alloy that consists of almost entirely α_2 phase in the whole temperature interval. Shear and transgranular brittle fracture together with some shallow dimples on the planar facets can be observed on the fracture surface of the specimen tested at room temperature (Fig. 7a). At 500°C fracture exhibits pure shear mode, characteristic for the cph crystals showing faceted

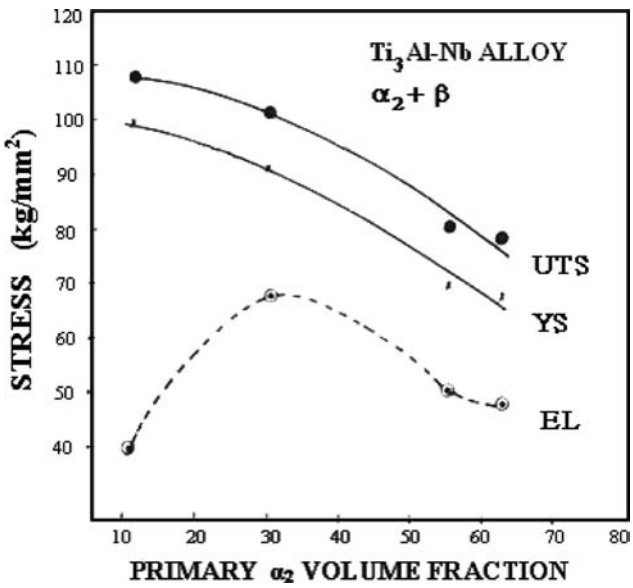

Figure 6 Tensile properties as a function of primary α_2 fraction in $\alpha_2 + \beta$ quenched samples [10].

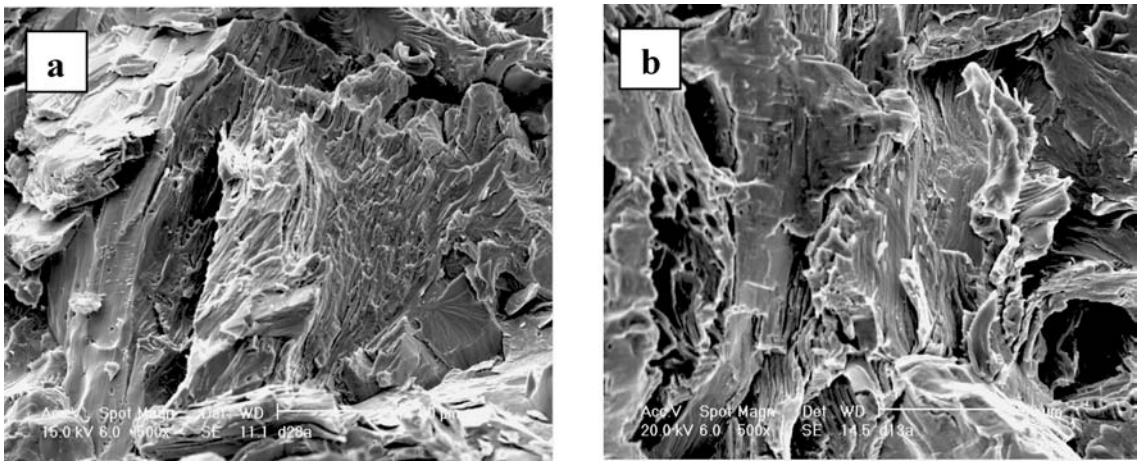

Figure 7 Fractography of the Ti_3Al alloy at (a) room temperature and (b) 500°C.

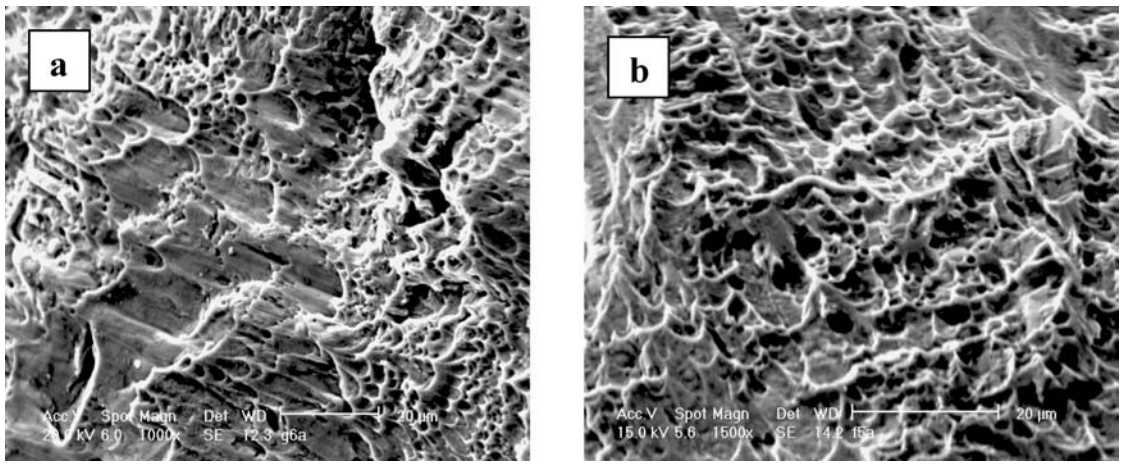

Figure 8 Fractography of the Ti_3Al-Nb alloy at (a) room temperature and (b) 500°C.

TABLE IV. Volume fraction of phases present in the microstructure of solution treated Ti_3Al based alloys

	Volume fraction (*vol.%*)	
Intermetallics	α_2	β
$Ti_3Al_{1050°C}$	96,21	3,79
$Ti_3Al\text{-}Nb_{1050°C}$	34,61	65,39
$Ti_3Al\text{-}Nb\text{-}Mo_{1050°C}$	21,73	78,27

transgranular brittle fracture with tearing on the steps joining the facetes (Fig. 7b). The lowest value of ductility of this alloy is the direct consequence of the transgranular brittle mode of fracture, since no plastic flow precedes the fracture.

In the case of Ti_3Al-Nb and Ti_3Al-Nb-Mo alloys, which structure consists of the α_2 and retained β phase, mixed fracture modes are operative both on the room and elevated temperatures (Fig. 8a,b), with the ductile fracture as a dominating mechanism. Since the fracture behavior of these two alloys is the same, only fracture surface of Ti_3Al-Nb will be presented. At the room temperature (Fig. 8a), these two alloys exhibit a combined transgranular fracture, which is mainly ductile and is characterized by microvoid coalescence and the presence of dimples, and faceted shear fracture dominated by slip decohesion. Fracture mechanism changes with increase in temperature (Fig. 8b) in the way, that the share of the ductile fracture increases which correlates with increase in ductility with temperature rise. Higher values of ductility in the case of Ti_3Al-Nb and Ti_3Al-Nb-Mo compared to Ti_3Al are the consequence of the presence of the ductile β phase and the ductile fracture as the prevailing fracture mechanism.

4. Conclusions

1. Mechanical alloying of the original starting Ti_3Al powder with Nb and Mo powders was achieved through ball-milling for 24 h, which is proven by the X-ray diffraction and EDS analysis. The powders were compacted by hot-pressing to non-porous homogenous compacts.

2. SEM revealed that the structure of pure Ti_3Al consists of the α_2 phase formed by $\beta \rightarrow \alpha \rightarrow \alpha_2$ transformation sequence. A two-phase ($\alpha_2 + \beta$) Widmanstätten microstructure is present in Ti_3Al-Nb and Ti_3Al-Nb-Mo alloys with fine α_2 lamellae in the β matrix.

3. The ultimate compression strength of each material increases with increasing test temperature, up to a maximum at 250°C, then a decrease occurs. Addition of Mo to Ti_3Al-Nb alloy yields the highest ultimate compression strength. The Ti_3Al-Nb alloy exhibits the highest ductility in the whole temperature range.

4. A correlation between ductility and the fracture mode exists for all materials. The minimum ductility level of Ti_3Al alloy corresponds to transgranular brittle mode of fracture at room and elevated temperatures. In the case of Ti_3Al-Nb and Ti_3Al-Nb-Mo alloys, ductile fracture mode dominates throughout the whole temperature interval, increasing their ductility compared to the pure Ti_3Al, as an effect of the presence of the retained β phase.

Acknowledgement

Authors are indebted to the Ministry of Science and Environment Protection of the Republic of Serbia for the financial support. Ti_3Al powder was kindly supplied by Max-Planck Institute für Metallforschung, Stuttgart, Germany.

References

1. C. H. CAO, J. M. MA and M. G. JAN, *Mat. Eng.* **2** (1991) 32.
2. Y. WU, I. ZHEN and D. Z. YANG, *Mat. Letters* **32** (1977) 319.
3. A. H. POSENSTEIN, *Mat. Sci. Eng.* **143A** (1991) 31.
4. S. DJANARTHANY, J. C. VIALA and J. BOUIX, *Mat. Chem. Phys.* **72** (2001) 301.
5. J. N. WANG, A. J. SCWARTZ, T. G. NIEH, C. T. LIU, V. K. SIKKA and D. CLEMENSIN, in: "*Gamma Titanium Aluminides*", ed. Z. W. KIM et al., TMS, Warrendale (1995) 949.
6. L. M. HSIUNG, T. G. NIEH and D. R. CLEMENS, *Scripta Mater.* **36** (1997) 233.
7. Y. UMIKOSHI, T. NAKANO and B. OGAWA, *Sripta Mater.* **34** (1996) 1161.
8. Đ. DROBNJAK, "*Physical Metallurgy*" (on Serbian), publication of TMF, Belgrade (1981).
9. R. G. ROWE, "*High Temperature Aluminides and Intermetallics*", Publication of TMS, Indianapolis (1989) 375–403.
10. A. K. GOGIA, D. BANERJEE and T. K. NANDY, *Metall. Trans.*, A **21** (1990) 609.
11. R. TRICOT, *Matér. Tech.* **76** (1988) 47.

Received 2 February
and accepted 14 November 2005